Direct Imaging of Exoplanets: Science and Techniques
Proceedings IAU Colloquium No. 200, 2005
C. Aime and F. Vakili, eds.

doi:10.1017/S1743921306009574

Visible Nulling Coronagraphy for Exo-Planetary Detection and Characterization

Richard G. Lyon, Mark Clampin[1], Robert Woodruff[2], Gopal Vasudevan[3], Mike Shao, Martin Levine[4], Gary Melnick, Volker Tolls[5], Peter Petrone, Peter Dogoda[6], Julia Duval[7], and Jian Ge[8]

[1]NASA/Goddard Space Flight Center, Greenbelt, MD
email:Richard.G.Lyon@nasa.gov, 301-286-4302

[2]Lockheed-Martin, Civil Space, Denver, CO

[3]Lockheed-Martin, Advanced Technology Center, Palo Alto, CA

[4]NASA/Jet Propulsion Laboratory, Pasadena, CA

[5]Harvard/SAO Center for Astrophysics, Cambridge, MA

[6]Sigma Space, Lanham, MD

[7]CNES, France

[8]University of Florida

Abstract. Visible Nulling Coronagraphy (VNC) is the proposed method of detecting and characterizing exo-solar Jovian planets (null depth 10^{-9}) for the proposed NASA's Extrasolar Planetary Imaging Coronagraph (EPIC) Clampin & Lyon 2004 and is an approach under evaluation for NASA's Terrestrial Planet Finder (TPF) mission. The VNC approach uses a single unobscured filled-aperture telescope and splits, via a 50 : 50 beamsplitter, its re-imaged pupil into two paths within a Mach-Zender interferometer. An achromatic PI phase shift is imposed onto one beam path and the two paths are laterally sheared with respect to each other. The two beams are recombined at a second 50 : 50 beamsplitter. The net effect is that the on axis (stellar) light is transmitted out of the bright interferometer arm while the off-axis (planetary) light is transmitted out of the nulled interferometer arm. The bright output is used for fine pointing control and coarse wavefront control. The nulled output is relayed to the science camera for science imagery and fine wavefront control. The actual transmission pattern, projected on the sky, follows a θ^2 pattern for a single shear, θ^4 for a double shear, with the spacing of the successive maxima proportional to the inverse of the relative lateral shear. Combinations of shears and spacecraft rolls build up the spatial frequency content of the sky transmission pattern in the same manner as imaging interferometer builds up the spatial frequency content of the image.

Keywords. Nulling coronography – exo-solar planets.

1. Introduction

The VNC approach has some significant advantages over more conventional mask coronagraphic approaches in that (i) its inner working angle is $2\lambda/D$ (assuming a 25% shear) allowing a smaller aperture than conventional coronagraphic methods that typically work at $4\lambda/D$, (ii) it has significantly less sensitivity to low order amplitude and wavefront aberrations – the shear is approximately equivalent to a lateral wavefront derivative which gives an f^2 multiplier on the wavefront PSD, thereby allowing for significantly lower quality optics in the telescope, (iii) coupling of the VNC nulled beams to a fiber bundle with a lenslet array on the front and back sides and a faceted micro-mirror array (MMA) within the nuller, with each MMA facet matched to each fiber, gives direct simultaneous

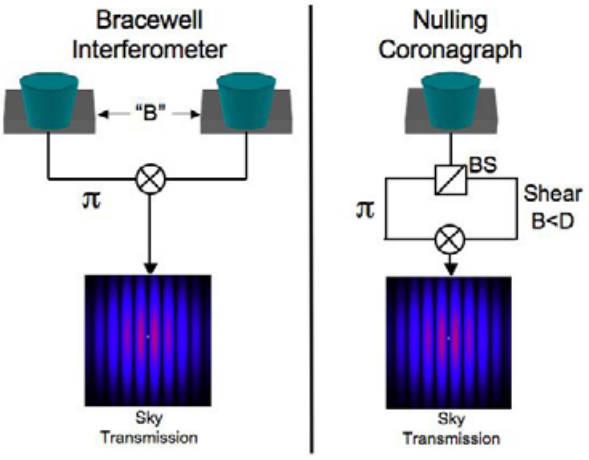

Figure 1. Bracewell and Visible Nulling Interferometer.

correction of both amplitude and phase with a single MMA per nuller, and, each fiber is a natural spatial filter on higher order wavefront errors. This also has a significant advantage in that focal plane mask errors in a conventional coronagraph are dispersive in the following pupil plane, making it difficult for any pupil plane deformable mirror to correct mask errors.

2. Principle of Visible Nulling Coronograph

Figure 1 shows simplified schematics of a Bracewell Nulling Interferometer (BNI) and a Visible Nulling Coronagraph (VNC). In a canonical BNI configuration 2 telescopes, separated by a baseline of B, are coherently interfered with a π phase shift giving a sky transmission, projected on the sky of $T^{\{2\}} = sin^2\left(\pi\frac{B}{\lambda}\theta\right) \sim \theta^2$ where θ is the sky angle in the direction of the baseline and λ is the wavelength. In a VNC the same pattern also arises except that B is now the relative pupil shear.

A VNC effectively emulates a BNI with only a single aperture. The condition for central nulling is given by

$$\sum_{j=1}^{N} e^{i\,\Phi_j} = 0$$

where Φ_j represents the relative phase shift due to the j^{th} aperture in the BNI and represents the j^{th} shear in VNC for a given set of N apertures or shears.

Figure 2 shows a conceptual optical configuration for a double sheared VNC, which is first sheared in the X direction followed by a shear in the Y direction. Light from the optical telescope assembly (OTA) is incident on a 50 : 50 beamsplitter which splits it into two paths. Light from the upper path (shown in red on top of Figure 2) reflects off a 90° corner reflector of which one mirror is a multiple mirror array (MMA) (Figure 3) and through two glass plates and to a second beam splitter. The MMA consists of MEMS based array of flat micro-mirrors, each movable in piston, tip and tilt. Light traverses the lower path (blue on top figure in Figure 2) after the first beamsplitter and reflects off a 90° corner reflector mounted on a two degree of freedom translation stage. This stage

https://doi.org/10.1017/S1743921306009574 Published online by Cambridge University Press

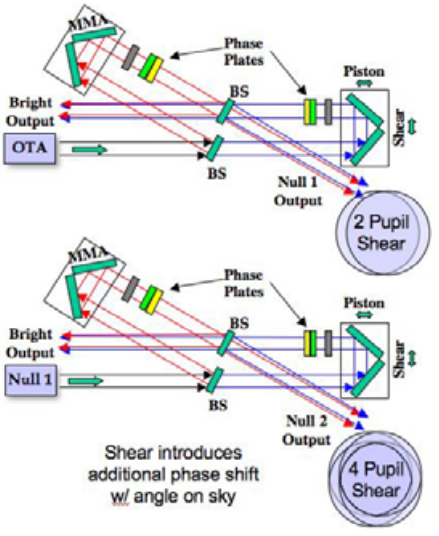

Figure 2. X/Y VNC Configuration.

can be moved in piston and to shear the lower paths beam with respect to the upper paths beam. The two beams are recombined at the second beamsplitter.

Setting the piston to yield a π phase shift allows the on-axis light to pass out through the bright output and the off-axis light to pass through to the nulled output. At the nulled output the two beams are laterally sheared which also introduces an additional phase shift resulting in nulling of the on-axis light (star) and transmission of off-axis light (planet). The output of the "X" nuller is fed into a second nuller which shears the beams orthogonal to the first nuller's shear direction, i.e. the "Y" direction and results in 4 sheared beams as shown in the lower right of Figure 2.

The output of the second nuller is passed into a spatial filter array (SFA) consisting of an array of lenslets, followed by an array of fibers and again by an array of lenslets, one lenslet per fiber (Figure 4). The net effect of the SFA is to allow correction of both amplitude and phase errors. From the two nullers are 4 sheared beams, overlaid, at the entrance aperture of the spatial filter array. The lenslet array divides the pupil into ~1200 hexagonal sub-apertures and thus 4 beamlets, each with relative phase shifts and amplitude shifts are injected into each fiber. At the output of each fiber it is desired that no light emerges. If light is observed at the output then the 2 MMA facets which are mapped to a given lenslet/fiber combination are moved in piston, tip and tilt. Moving

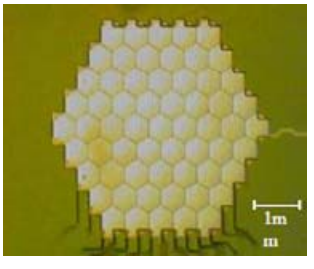

Figure 3. MMA.

https://doi.org/10.1017/S1743921306009574 Published online by Cambridge University Press

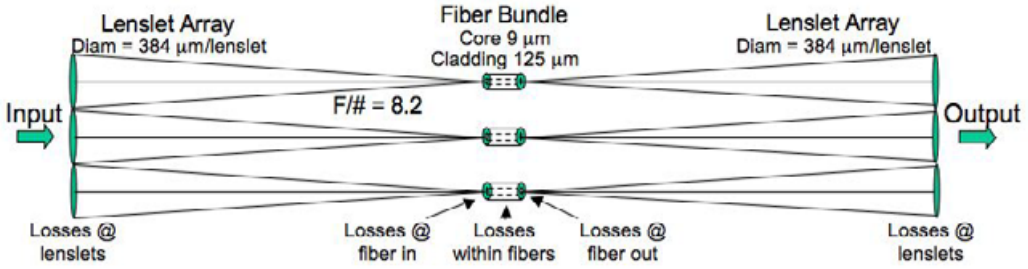

Figure 4. Schematic of SFA.

each MMA facet in piston compensates for non-common path length errors introduced in the two nullers to effectively main the condition for central nulling. Motion of the MMA facets in tip/tilt steer the sub-aperture point spread function (PSF) on the ends of the fibers. Since there is a MMA in only one arm of each of the two nullers, one can in principle always match the amplitudes. Thus the combination of the SFA and MMA correct for amplitude and phase errors.

Figure 5 shows a simulation of the intensity entering the input lenslet array of the SFA (left side) and the intensity entering the fiber bundle. Note that there is one MMA micro-mirror per lenslet/fiber. The speckled pattern is due to residual wavefront errors from the OTA and non-common path errors introduced in the X and Y nullers.

Light injected into a fiber will ultimately evolve into an eigenmode of the fiber. At the fiber output, independent of the functional form of the input field, the output can be characterized by only amplitude and phase. The planetary light, entering the OTA slightly off-axis, but within the numerical aperture of the fiber, will emerge with a stairstep phase as shown on the rightside of Figure 6. The net effect is that the fiber bundle coupled to the lenslets will cause grating like sidelobes in the planet image, rightside of Figure 6. The sidelobes are periodic and will occur at angular sky spacings of $\sim N \times \lambda/D$, where N is the number of fibers across a diameter of the bundle, λ is the wavelength of light and $D$is the OTA entrance aperture diameter. These sidelobes effectively limit the field of view of the VNC and result in $\sim$2% loss in the planetary flux.

The effective planetary sky transmission pattern is built up from several spacecraft rolls and several shears of the VNC. Figure 7 shows an example of a possible transmission patter with 3 rolls of 0, 15 and 30 degrees and 4 shear combinations for a passband of 90 nm centered on 600 nm. It can be see that with a relatively small number of shear/roll combinations high contrast transmission is possible through the planetary search space. Figure 8 a simulation of a Jupiter and Saturn planetary detection.

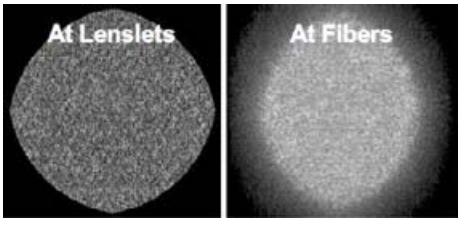

Figure 5. Simulation of Intensity entering SFA lenslet array and at fiber bundle entrance.

https://doi.org/10.1017/S1743921306009574 Published online by Cambridge University Press

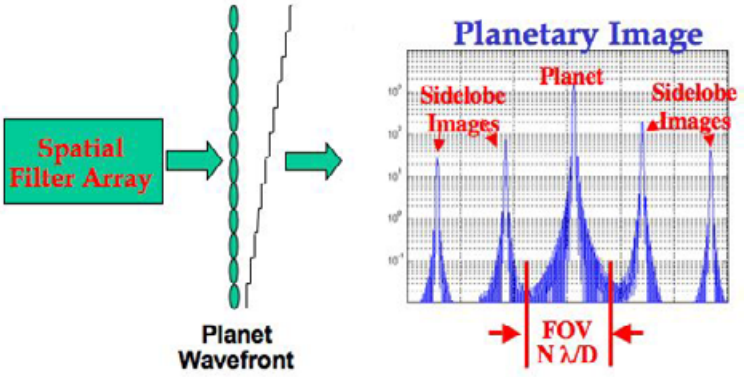

Figure 6. Planetary Image.

3. VNC Sensitivities and Initial Error Budgeting

For the X and Y shear configuration for an resolved stellar on-axis source the scalar electric field at the output of the 2 nullers can be represented as:

$$E_T(x,y) = \approx t\frac{E_0}{4}\sum_{j=1}^{4}(-1)^{j-1}\left(1+\delta A_j(x,y)\right)\left(1+i\Phi_j(x,y)\right) \tag{3.1}$$

where we have expanded to first order the phase and amplitude variations and "t" represents the throughput. Assuming ensemble averages over uncorrelated Gaussian statistics yields for the intensity:

$$I_T(x,y) \approx \frac{1}{16}PSF_0(\theta)\left[\sum_{j=1}^{4}\left\langle \mid \delta A_j(\theta)\mid^2\right\rangle_{\delta A} + \sum_{j=1}^{4}\left\langle \mid \Phi_j(\theta)\mid^2\right\rangle_{\Phi}\right] \tag{3.2}$$

where θ represents the angle on the sky and the angled brackets represent ensemble averages. PSF_0 is the point spread function without errors. If we assume an asymptotic form for the error free point spread function and evaluate the ensemble averaged terms in equation 3.2 for a linearly filtered random process then 3.2 can be evaluated in terms

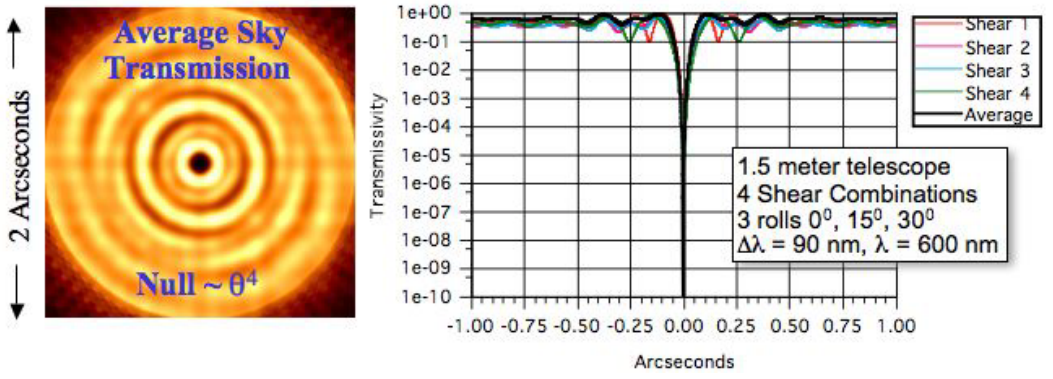

Figure 7. Sky Transmission Pattern.

https://doi.org/10.1017/S1743921306009574 Published online by Cambridge University Press

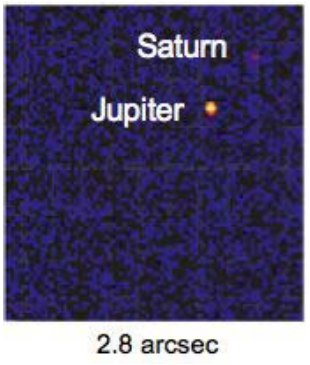

Figure 8. Simulated Jupiter/Saturn Detection.

of power spectral densities to yield:

$$I_{Star}(\theta) \approx \frac{1}{16} \frac{L_{Star}}{1+\frac{\pi^4}{8}\theta^3} \left[\left(\sigma^2_{N1,\delta A} + \sigma^2_{N2,\delta A}\right) PSD_{\delta A}(\theta) + \left(\sigma^2_{N1,\Phi} + \sigma^2_{N2,\Phi}\right) PSD_{\Phi}(\theta) \right] \tag{3.3}$$

where L_{Star} represents the stellar luminosity, θ the sky angle in units of λ/D, and $\sigma_{N1,\delta A}$, $\sigma_{N2,\delta A}$ represent the fractional rms amplitude errors in nullers 1 and 2 respectively and $\sigma_{N1,\Phi}$, $\sigma_{N2,\Phi}$ the rms phase errors (in radians) in nullers 1 and 2 respectively. In the above formalism the asymptotic PSF, $\left[1+\frac{\pi^4}{8}\theta^3\right]^{-1}$ is normalized to unity at the origin as are the amplitude and phase error power spectral densities. Note that in equation 3.3 the error PSDs are multipliers on the stellar leakage, implying that for no errors no starlight gets through at any point in the focal plane.

The off-axis planetary light is given by:

$$I_{Planet}(\theta) = \frac{L_{Planet}}{1+\frac{\pi^4}{8}(\theta-\theta_p)^3} sin^2\left(2\pi S_x \theta_{xp}\right) sin^2\left(2\pi S_y \theta_{yp}\right) \tag{3.4}$$

where $\theta_p = (\theta_{xp}, \theta_{yp})$ is the planet location in units of l/D and (S_x, S_y) is the fractional pupil shear in the X and Y directions respectively. Note that the transmission pattern is a multiplier on the planets asymptotic PSF, but the coordinates of the transmission pattern depend on the location of the planet.

To calculate the contrast of the planet to the stellar leakage, at the location of the planet we only need to ration equation 3.4 to equation 3.3 and evaluate the result at the location of the planet to yield the contrast of:

$$Q = 16 \frac{L_{Planet}}{L_{Star}} \frac{1+\frac{\pi^4}{8}\theta_p^3}{\left[\left(\sigma^2_{N1,\delta A} + \sigma^2_{N2,\delta A}\right) PSD_{\delta A}(\theta_p) + \left(\sigma^2_{N1,\Phi} + \sigma^2_{N2,\Phi}\right) PSD_{\Phi}(\theta_p)\right]} \tag{3.5}$$

Equation 3.5 assumes that the nuller shears are set such that the sky transmission function is unity (shear matched condition). From 3.5 it is evident that Q is inversely proportional to the variances of the amplitude and phase errors and increases as approximately the 3^{rd} power of the planet to star angular separation.

Assuming that the error PSDs all have the form of $PSD(\theta) = \frac{1}{1+(\theta/\theta_{knee})}$ and assuming, e.g., that all the error occurs as phase (wavefront) error and solving equation 3.5 for the

https://doi.org/10.1017/S1743921306009574 Published online by Cambridge University Press

error yields:

$$\sigma_T = 4\sqrt{\frac{1}{Q}\frac{L_{Planet}}{L_{Star}}\left(1+\frac{\pi^4}{8}\theta_p^3\right)\left(1+\left(\frac{\theta_p}{\theta_{knee}}\right)^3\right)} \tag{3.6}$$

Equation 3.6 is plotted in Figure 9, showing the total rms wavefront error, in units of waves, versus the desired inner working angle for three values of "Q". The planet to stellar luminosity ratio is assumed to be 10^{-10}. It is seen that a desired inner working angle of $4\lambda/D$ requires residual wavefront errors $\sim\lambda/500$ rms and an inner working angle of $2\lambda/D$ requires residual wavefront errors of $\sim\lambda/5000$ rms to detect terrestrial planets.

4. Lab Visible Nulling Coronograph

In order to realize the EPIC science mission the NASA technology readiness levels (TRL) of the VNC must be advanced enough to yield a stable achromatic (15% passband) null (10^{-9}) for 1000 seconds. In order to achieve this goal we have been developing a laboratory testbed (Figure 10). The testbed consists of a source module consisting of a fiber injected source reflecting off a thin 50 : 50 pellicle to an off-axis parabola (OAP), to a reflecting flat, back to the off-axis parabola and transmitting through the pellicle, to a small collimating off-axis parabola (left side of Figure 10) and into the lab VNC (rightside of Figure 10). The OAP and flat of the source module are specially designed and manufactured to comprise a matched pair such that where ever there is a bump/pit on the parabola there is a pit/bump on the flat Kestner & Witebsky 2004. The resultant wavefront quality from the source module is 1.2 nm rms wavefront error. The surface maps and combined maps of these optics are shown in Figure 11. Lateral translation of the flat, away from the ideal aligned position, allows control of the wavefront error from $\sim\lambda/500$ to $\sim\lambda/20$ to demonstrate holding of the null while varying wavefront errors.

5. Summary and Conclusions

The VNC approach has some significant advantages over more conventional mask coronagraphic approaches in that (i) its inner working angle is $\sim 2\lambda/D$ (assuming a 25%

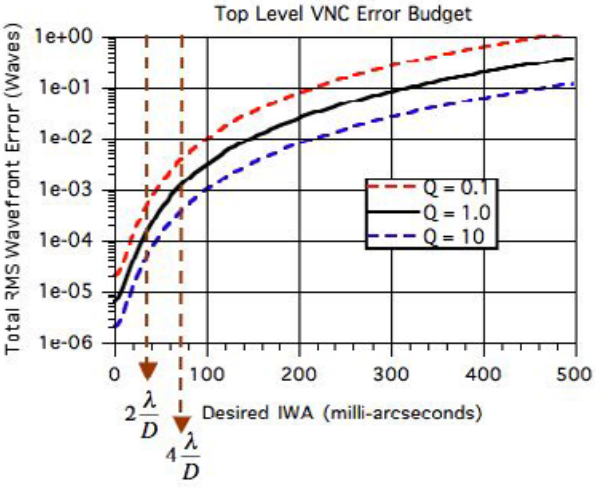

Figure 9. RMS WFE vs IWA.

https://doi.org/10.1017/S1743921306009574 Published online by Cambridge University Press

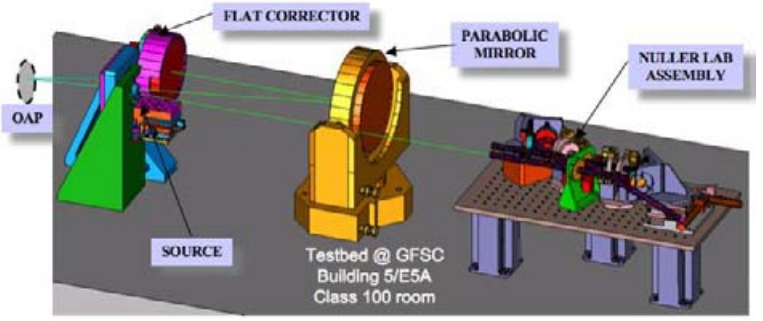

Figure 10. Visible Nulling Coronagraph.

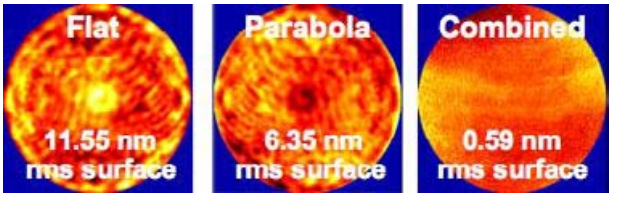

Figure 11. Source Module Surface Maps.

shear) allowing a smaller aperture than conventional coronagraphic methods that typically work at $\sim 4\lambda/D$, (ii) it has significantly less sensitivity to low order amplitude and wavefront aberrations – the shear is approximately equivalent to a lateral wavefront derivative which gives an f2 multiplier on the wavefront PSD, thereby allowing for significantly lower quality optics in the telescope, (iii) coupling of the VNC nulled beams to a fiber bundle with a lenslet array on the front and back sides and a faceted micro-mirror array (MMA) within the nuller, with each MMA facet matched to each fiber, gives direct simultaneous correction of both amplitude and phase with a single MMA per nuller, and, each fiber is a natural spatial filter on higher order wavefront errors. This also has a significant advantage in that focal plane mask errors in a conventional coronagraph are dispersive in the following pupil plane, making it difficult for any pupil plane deformable mirror to correct mask errors.

References

M. Clampin, R. G. Lyon, G. Melnick, P. Nisenson, R. A. Woodruff, M. Harwit, D.Y. Gezari, L. Petro, H. Ford, R. Mauk, H. Smith, *The Extra-solar Planetary Imaging Coronagraph*, Proceedings of SPIE 5487, Glasgow Scotland, June 21–25, 2004

Kestner, R., Witebsky, C., Clampin, M. Lyon, R., Woodruff, R., Irregulary Figured Plates Correct Wavefront Errors, Laser Focus World, Volume 40, Issue 12, December 2004

https://doi.org/10.1017/S1743921306009574 Published online by Cambridge University Press